Central-field model for the γ spectrum of positrons annihilating on rare-gas atoms

Yongjun Cheng[1,2,*] and J. Mitroy[2,†]

[1]*Academy of Fundamental and Interdisciplinary Science, Harbin Institute of Technology, Harbin 150080, P.R. China*

[2]*Centre for Antimatter-Matter Studies and School of Engineering, Charles Darwin University, Darwin, Northern Territory 0909, Australia*

(Received 10 July 2014; published 6 October 2014)

A central field model is used to study the two-photon positron annihilation spectrum for the rare gas atoms He, Ne, Ar, Kr, and Xe at energies close to thermal. Correlation effects are incorporated with a semiempirical polarization potential. The γ spectrum is given, with values reported for individual subshells. The predicted full widths at half-maximum (FWHM) for all systems are typically 5%–20% larger than the experimental values reported using the positron trap at the University of California, San Diego, while, with the exception of neon, generally being 2%–10% smaller than the FWHMs measured at University College London. The detailed spectrum for xenon is reported and the likelihood of core annihilation's making a measurable contribution to the observed Doppler spectrum is discussed. The γ spectra are found to be insensitive to variations in the scattering potential and whether the target is represented by a Hartree-Fock or a Dirac-Fock wave function. The model potential used in the solution of the positron-atom Schrödinger equation provides a reasonable fit to recent total elastic cross-section measurements reported by the Australian National University and University of Trento groups.

DOI: 10.1103/PhysRevA.90.042702 PACS number(s): 34.80.Uv, 36.10.−k, 78.70.Bj

I. INTRODUCTION

There are two types of collision processes possible when positrons with energies less than the positronium formation threshold of the target collide with a gas with an ionization potential greater than the positronium binding energy of 6.8 eV. The first process is elastic scattering, where the positron is deflected by the potential field of the atom. The second process is positron annihilation, where the positron comes in contact with one of the atomic electrons and subsequently emits γ radiation. The most usual annihilation process is the 2γ event, where two photons, each with an energy of almost 511 keV, are emitted. Both elastic scattering and positron annihilation are dependent on the response of the atom to the incoming position; the positron distorts the atomic charge cloud, and this distortion greatly influences both collision processes.

This work is focused on the investigation of the dynamics of positron annihilation from rare gases in a central field model. When a positron and an electron annihilate at rest, the outcome is the emission of 2γ rays at an angle of exactly 180°. However, when the collision occurs in the atomic environment, both the electron and the positron carry momentum and this leads to the 2γ photons being emitted at a laboratory frame angle that is slightly different from 180°. In addition, there is also a Doppler shift that leads to the energy of the γ photons being different from 510.9989 keV.

The γ spectrum of the annihilating radiation does reveal additional information about the nature of the collision, just as the differential cross section gives additional information on the nature of elastic scattering collisions. For this reason, there have been a number of experimental and theoretical investigations of the γ radiation emitted when positrons annihilate with noble gases. There have been four studies on the experimental side [1–4]. Three of these investigations have been performed in the traditional configuration [1,3,4]. High-energy positrons from a source are emitted into a gas, and the total annihilation rate and γ spectrum are determined once the positrons have thermalized. The fourth experiment was performed in a positron trap. In the trap configuration, pioneered by the group at the University of California, San Diego (UCSD) [2,5,6], positrons are first cooled in a buffer gas (usually N_2), and once the positrons have thermalized a target gas is introduced and the annihilation rate and profile are measured.

On the theoretical side, one can point to investigations using the polarized orbital (PO) approach [7–11] and an approach based on quantum chemistry techniques [12,13]. There have been three many-body perturbation theory (MBPT) calculations, all of which have Gribakin in the author list [14–16]. These MBPT calculations are identified by adding a suffix identifying the year of publication; e.g., MBPT96 refers to the calculation by Dzuba *et al.* [15], while MBPT14 refers to the most recent calculation [14]. There have also been some high-accuracy calculations using correlated basis sets for positrons annihilating with hydrogen and helium atoms [17–22].

The present article uses a central field model to calculate the annihilation spectrum for low-energy positrons colliding with rare gas atoms, with emphasis on the full width at half-maximum (FWHM). The contribution of core annihilation to the annihilation spectrum of xenon is also discussed. All calculations are performed within a central field approximation. The advantage of this approach is that the calculations are not computationally expensive, which permits various dynamical aspects to be systematically investigated. The reliability of the model potential (MP) is tested by computing the elastic cross section below the positronium formation threshold and comparing it with experiment and other calculations. Being able to reproduce the accurate elastic cross section is a necessary but not sufficient condition for the reliability of the dynamical model. The previous calculation of Dunn *et al.* [23] has shown that a theoretical model may not be able to reproduce an accurate annihilation cross section even if an accurate elastic cross section can be obtained.

*cyj83mail@gmail.com

†Deceased.

II. FORMALISM

A. General formalism

For positron annihilating on an N electron atom, the final state will consist of an $N-1$ electron residual ion in a state ϕ_ν and a couple of γ rays with total momentum $\mathbf{q}=\mathbf{k}_0+\mathbf{k}_i$. $\mathbf{k}_0$ and $\mathbf{k}_i$ are the momentum of the positron and the electron participating in annihilation, respectively. The 2γ annihilation rate to such a final state is given [18] as

$$\Lambda_\nu(\mathbf{q}) = S\sum_{i=1}^{N}\left|\int\prod_{j=0}^{N} d^3r_j\ \phi_\nu^*(\mathbf{r}_1,\ldots,\mathbf{r}_{i-1},\mathbf{r}_{i+1},\ldots,\mathbf{r}_N) \times \frac{e^{i\mathbf{q}\cdot\mathbf{r}_0}}{(2\pi)^{3/2}}\hat{O}_i^S\delta(\mathbf{r}_i-\mathbf{r}_0)\Psi(\mathbf{r}_1,\ldots,\mathbf{r}_N;\mathbf{r}_0)\right|^2. \quad (1)$$

The coordinate $\mathbf{r}_0$ in Eq. (1) denotes the positron, $\Psi(\mathbf{r}_1,\ldots,\mathbf{r}_N;\mathbf{r}_0)$ is the initial wave function of the positron-atom system, and S is a constant defined to lowest order as

$$S = 4\pi c\alpha^4 a_0^2, \quad (2)$$

where c is the speed of light, α is the Bohr radius, and a_0 is the fine-structure constant. The operator $\hat{O}_N^S$ is a spin projection operator to the positron–(Nth electron) pair, which can be written as

$$\hat{O}_N^S = 1-\tfrac{1}{2}S^2_{e_N,p}. \quad (3)$$

Using the antisymmetry of the initial wave function of the system to set the index of the annihilating electron as $i=N$ and summing over all the possible final states of the residual ion, Eq. (1) yields a quantity $\Gamma(\mathbf{q})$, termed the 2γ annihilation rate [7,24]:

$$\Gamma(\mathbf{q}) = \sum_{\mu=1} SN_\mu\int d^3r_1\ldots d^3r_{N-1} \times\left|\int d^3r_N\frac{e^{i\mathbf{q}\cdot\mathbf{r}_N}}{(2\pi)^{\frac{3}{2}}}\hat{O}_N^S\Psi(r_1,\ldots,r_N;r_N)\right|^2. \quad (4)$$

Here N_μ is the number of electrons in the shell of the atom where the annihilation electron exists. The 2γ annihilation rate $\Gamma(\mathbf{q})$ describes the annihilation rate to a final state where γ rays have a total momentum of $\mathbf{q}$.

Based on Eq. (4) the γ spectrum for positron annihilation, an important quantity that can be measured in experiments to study the momentum distribution of the annihilating electron-positron pair, is represented as [25]

$$W(E) = \frac{1}{c}\int\int\int_{\frac{2E}{c}}^{\infty} q\Gamma(\mathbf{q})\frac{dqd\Omega}{(2\pi)^3}, \quad (5)$$

where $E=E_\gamma-510.9989$ keV is the energy deviation of the γ ray relative to m_ec^2 due to Doppler broadening. This quantity is also termed the angular correlation if a relation between the energy deviation E and the angle between the two γ rays, θ, is applied [17]:

$$E = m_ec^2\frac{\theta}{2}. \quad (6)$$

The annihilation parameter, $Z_{\rm eff}$, is the effective number of electrons participating in annihilation. This can be calculated as [26]

$$Z_{\rm eff} = N\int|\Psi(r_1,\ldots,r_N,r_N)|^2d^3r_1\ldots d^3r_N. \quad (7)$$

When the plane-wave Born approximation (PWBA) or a central field model was applied, the wave function of the system $\Psi(r_1,\ldots,r_N,r_N)$ could be represented as the product of the wave function of the atom $\Phi(r_1,\ldots,r_N)$ and the wave function of the positron, $\psi(\mathbf{k},r)$. Then the expression for $Z_{\rm eff}$ is given as [24]

$$Z_{\rm eff} = N\int|\Phi(r_1,\ldots,r_N)\psi(\mathbf{k},r_N)|^2d^3r_1\ldots d^3r_N. \quad (8)$$

The positron wave function is $\psi(\mathbf{k},r)=(2\pi)^{-3/2}\exp(i\mathbf{k}\cdot\mathbf{r})$, in the PWBA, and $Z_{\rm eff}$ is equal to the number of electrons N.

In the present article, the γ spectrum and the annihilation parameter, $Z_{\rm eff}$, for positron annihilation from the noble gas atoms He, Ne, Ar, Kr, and Xe are computed within a central field model. Expressions of $\Gamma(\mathbf{q})$ are given in the following sections.

B. Plane-wave Born approximation

In the calculation with the PWBA, the wave function of the system is expressed as the product of a plane wave for the positron and a Hartree-Fock (HF) wave function for the atom. Then the quantity $\Gamma(\mathbf{q})$ is calculated as

$$\begin{aligned}\Gamma(\mathbf{q}) &= \sum_{\mu=1} SN_\mu\left|\int d^3r\frac{e^{i\mathbf{q}\cdot\mathbf{r}}}{(2\pi)^{\frac{3}{2}}}\hat{O}^S\Phi_\mu(r)e^{ik_0\cdot r}\right|^2\\ &= \sum_{\mu=1}\frac{SN_\mu}{2\ell_\mu+1}\sum_{m_\mu}\left|\int d^3r\frac{e^{i\mathbf{k}\cdot\mathbf{r}}}{(2\pi)^{\frac{3}{2}}}\hat{O}^S\Phi_\mu(r)\right|^2,\\ \mathbf{k} &= \mathbf{q}+\mathbf{k}_0. \end{aligned} \quad (9)$$

Applying the partial-wave expansion for the plane wave, one can get the expression for $\Gamma(\mathbf{q})$ as follows:

$$\Gamma(\mathbf{q}) = \sum_{\mu=1}\frac{SN_\mu}{8\pi^2}\left|\int r^2\phi(r)j_{\ell_\mu}(kr)dr\right|^2. \quad (10)$$

$j_{\ell_\mu}(kr)$ is the spherical Bessel function. The PWBA can be evaluated with or without a partial-wave expansion of the scattering wave function. This permits an independent numerical validation of the distorted-wave calculations, which require a partial-wave expansion of the scattering wave function.

C. Central field model

1. Scattering potential

In the present central field model, the total wave function was produced within the distorted-wave approximation with a semiempirical model potential adopted to describe the polarization effect. A Numerov method was used to integrate the Schrödinger equation from the origin to the asymptotic boundary and the phase shift and normalization were

TABLE I. Scattering lengths (in a_0) for positron scattering from noble gas atoms. MP model scattering lengths were determined from the phase shifts at $k = 0.001\ a_0^{-1}$ and should be numerically reliable to better than 1%.

	He	Ne	Ar	Kr	Xe
Present MP	−0.49	−0.61	−5.28	−10.2	−56
PO [7–11]	−0.53	−0.61	−5.3	−10.4	−45
MBPT96 [15]		−0.43	−3.9	−9.1	≈−100
MBPT14 [14]	−0.435	−0.467	−4.41	−9.71	−84.5(2)
CCC [27]		−0.53	−4.3	−11.2	−117
Kohn [28]	−0.48				
Expt. (Trento)			−4.9 ± 0.7 [29]	−10.3 ± 1.5 [30]	−99.2 ± 18.4 [31]
$\langle Z_{\rm eff}\rangle_T$ [24,32]			≈−5.6	≈−10.3	≈−56

determined by matching the numerical wave function with the asymptotic form of the scattering wave function.

The effective Hamiltonian for a positron moving in the field of an atom is written

$$H = -\tfrac{1}{2}\nabla_0^2 + V_{\rm dir}(\mathbf{r}_0) + V_{\rm pol}(\mathbf{r}_0). \tag{11}$$

The direct interaction $V_{\rm dir}$ between the positron and the target was calculated exactly. The target wave function was taken from an HF calculation using a Slater-type orbital basis.

The semiempirical polarization potential, $V_{\rm pol}(r_0)$, had the functional form

$$\begin{aligned} V_{\rm pol}(r_0) = &-\frac{\alpha_d\left[1-\exp\left(-r_0^6/\rho^6\right)\right]}{2r_0^4} \\ &-\frac{\alpha_q\left[1-\exp\left(-r_0^8/\rho^8\right)\right]}{2r_0^6} \\ &-\frac{\alpha_o\left[1-\exp\left(-r_0^{10}/\rho^{10}\right)\right]}{2r_0^8}. \end{aligned} \tag{12}$$

The coefficients, α_d, α_q, and α_o are the static dipole, quadrupole, and octupole polarizabilities, respectively. The cutoff parameter, ρ, was tuned to reproduce the scattering length (or a phase shift) from an external source. The external source could be an experiment or an *ab initio* calculation. Available information for the scattering lengths of positron scattering with noble gas atoms is listed in Table I. The multipole polarizabilities adopted in the present calculations and the scattering lengths used to tune the cutoff parameters are tabulated in Table II. We present three calculations of the positron annihilation spectra in this paper. The first calculation just uses the total interaction potential of $V(r) = 0$ and is the PWBA. The next calculation sets $V_{\rm pol}(r) = 0$ and is termed the static calculation. The calculation using Eq. (12) is called the MP calculation.

TABLE II. Dipole α_d, quadrupole α_q, and octupole α_o polarizabilities adopted in our calculations are tabulated. These multipole polarizabilities are taken from [24], [40], and [57–59]. Scattering lengths, A, used to tune the calculations and enhancement factors are also listed.

	He	Ne	Ar	Kr	Xe
α_d	1.383	2.67	11.10	16.80	27.30
α_q	2.40	7.52	52.80	98.20	213.7
α_o	10.62	42.07	536.4	1273	3646
A	−0.48	−0.61	−5.28	−10.2	−56
$G_{\rm core}$		1.24	1.45	1.77	1.93
$G_{\rm val}$	3.188	2.813	3.876	5.479	8.621

The present MP calculation is a refinement over an earlier central field investigation of positron scattering which included only the dipole part of the polarization potential [24]. The reasons for the inclusion of additional terms is based on theoretical and pragmatic considerations. First, the quadrupole and octupole parts are necessary for a better description of the polarization potential, especially for the heavier rare gas atoms, which have larger polarizabilities. The attractive electron-positron interaction leads to clustering of the electron and positron into a composite entity resembling a positronium. This clustering manifests itself in a polarization potential for which terms beyond dipole excitations are important [33–36]. The second justification is based on comparisons with large-scale *ab initio* calculations of positron scattering from Mg, Cu, and Zn. A potential model going beyond purely dipole potentials was better able to reproduce the energies obtained from the *ab initio* calculations [37]. The number of terms in Eq. (12) was restricted to three since high-quality calculations of the noble gas polarizabilities usually terminate at the octupole polarizability [38–40].

The three-term polarization potential does have a significantly different shape than the one-term polarization potential does. Figure 1 shows the one-term (i.e., dipole only) and three-term polarization potentials for positron-argon scattering. Both polarization potentials have been tuned to give the same scattering length, $-5.28\ a_0$. The three-term potential is shallower than the one-term potential but larger in the outer valence region. The use of the three-term polarization (instead of the one-term potential) did lead to some changes in the energy dependence of the elastic cross section and some other properties. The changes in going from a one-term to a two-term potential were about a factor of 5 larger than the changes resulting from a two-term to a three-term potential.

2. *Positron annihilation*

The annihilation rate $\Gamma(\mathbf{q})$ can be computed from the positron distorted wave function $\psi(\mathbf{k},r)$ using

$$\Gamma(\mathbf{q}) = \sum_{\mu=1} SN_\mu \left| \int d^3r \frac{e^{i\mathbf{q}\cdot\mathbf{r}}}{(2\pi)^{\frac{3}{2}}} \hat{O}^S \Phi_\mu(r)\psi(\mathbf{k},r) \right|^2. \tag{13}$$

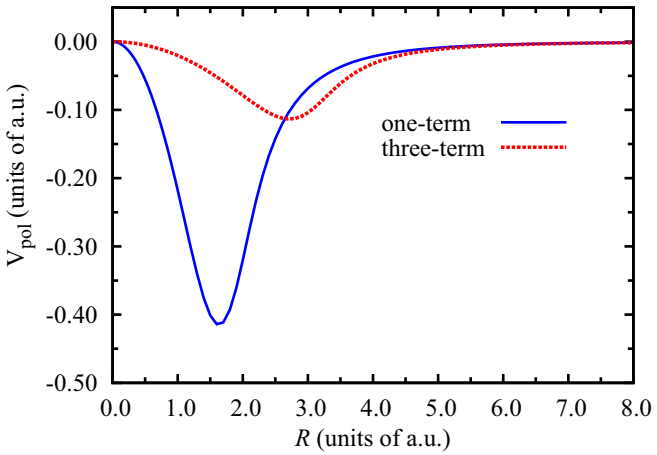

FIG. 1. (Color online) Two polarization potentials for positron-argon scattering. Both were tuned to have the same scattering length, $-5.28\ a_0$.

Making a partial-wave expansion gives

$$\Gamma(\mathbf{q}) = \sum_{\mu=1}\sum_{m_\mu}\frac{SN_\mu}{2\ell_\mu+1}\left|\int d^3r\,\frac{e^{i\mathbf{q}\cdot\mathbf{r}}}{(2\pi)^{\frac{3}{2}}}\hat{O}^S\Phi_\mu(r)\psi(\mathbf{k},r)\right|^2$$

$$= \sum_{\mu=1}\sum_{m_\mu}\frac{SN_\mu}{8\pi^2}F_\mu F_\mu^*, \tag{14}$$

$$F_\mu = \sum_{\ell_1\ell_2}(2\ell_1+1)(2\ell_2+1)\mathrm{i}^{\ell_1+\ell_2}P_{\ell_2}(\cos\theta)$$

$$\times\begin{pmatrix}\ell_1 & \ell_2 & \ell_\mu\\ 0 & -m_\mu & m_\mu\end{pmatrix}\begin{pmatrix}\ell_1 & \ell_2 & \ell_\mu\\ 0 & 0 & 0\end{pmatrix}$$

$$\times\int\psi_{\ell_1}(kr)j_{\ell_2}(qr)\Phi_\mu(r)r^2dr, \tag{15}$$

$$\ell_2 = |\ell_1-\ell_\mu|,\ldots,\ell_1+\ell_\mu, \tag{16}$$

$$\ell_1+\ell_2+\ell_\mu = \text{even}. \tag{17}$$

The computational details were checked by integrating the Schrödinger equation for a 0 potential and then comparing the annihilation profile with that computed using Eq. (10). The most commonly used parameter to characterize the γ spectrum is the FWHM of the annihilation energy spectrum. This is computed by inserting $\Gamma(\mathbf{q})$ into Eq. (5) and calculating $W(E)$ for a grid of values.

D. Enhancement factors

Positron annihilation calculations using model potentials and the simple product wave functions are known to underestimate the annihilation rate. The strongly attractive electron-positron interaction leads to strong electron-positron correlations that increase the electron density at the position of the positron [36,41–43]. Consequently, multiplicative enhancement factors, G, are introduced to rescale the calculated annihilation rate. This can be done by multiplying the right-hand side of Eq. (14) by the enhancement factor, G.

One justification for the use of enhancement factors comes from an earlier semiempirical analysis of positron-gas scattering [36]. Calculations tuned to reproduce the scattering lengths from accurate *ab initio* calculations for hydrogen and helium were able to reproduce the energy dependence of the s-wave $Z_{\rm eff}(k)$ up to a multiplying factor (i.e., the enhancement factor) for energies below the Ps-formation threshold. In addition, a first-principles calculation of the enhancement factor for hydrogen showed an s-wave enhancement factor that was independent of energy up to the Ps-formation threshold [44]. The s-wave enhancement factor from this calculation was about 6.5. Using the methodology described in this work, we have also constructed a semiempirical model potential for atomic hydrogen by tuning to the positron-H scattering length [45]. The enhancement factor needed to reproduce $Z_{\rm eff}$ from variational calculations [46,47] was 6.87.

The enhancement factors G that were used in the present calculation were tuned to experimental values. In the previous work [24], the enhancement factor, G was the same for all target orbitals of a given atom. A more refined approach is adopted here since the present investigation touches on core annihilation. The extent of electron-positron clustering in the total wave function is known to depend on the orbital binding energy of the electron with which it is interacting [36,48,49]. The degree of clustering decreases as the binding energy of the atomic orbital increased. As the degree of clustering decreases, so do the enhancement factors [24,35,37,50–52].

Consequently, different enhancement factors are used for core and valence electrons, with the valence electrons chosen as the eight electrons in the most weakly bound ns and np orbitals. The core enhancement factor was fixed by using the empirical relation $G_{\rm core}\approx 1+1.4/\sqrt{E-0.52}$, where E is the binding energy (Koopmans energy) of the orbital. The dependency of the enhancement factor on the square root of the binding energy is suggested by the enhancement factors for positron annihilation on the hydrogenic ions [35,50]. This equation was determined by reference to the valence enhancement factors for neon and argon, the rare gases with the most tightly bound electrons. Since only less than 0.5% of the total annihilation rate for neon and argon comes from core annihilation, the enhancement factors for valence annihilation $G_{\rm val}$ would changed only slightly when the different enhancement factors for core annihilation $G_{\rm core}$ were adopted. First, we used a single value of enhancement factors for both core and valence electrons of neon and argon to reproduce the experimental estimates of $Z_{\rm eff}$ and determined the empirical relation between $G_{\rm val}$ and the binding energy E of the valence orbital. The value of E in the expression was the average of the ns and np Koopmans energies (in a.u.) weighted by the number of electrons in each subshell. Then we used this relation to fix $G_{\rm core}$ and adjusted $G_{\rm val}$ to reproduce the experimental estimates of $Z_{\rm eff}$. The new value of $G_{\rm val}$ was within 1% of its initial value, which was used to determine the empirical relation.

The core enhancement factors are listed in Table II. The accuracy of these enhancement factors should be about 25%. The core enhancement factors for Kr and Xe were estimated by using the orbital energies of the $(n-1)d$ orbitals in the approximate identity. The core enhancement factor for neon used the Koopmans energy of the $1s$ subshell. The

TABLE III. Thermally averaged values of $Z_{\rm eff}$, i.e., $\langle Z_{\rm eff}\rangle_T$, at 293 K for positron scattering from noble gases are listed. Values of $Z_{\rm eff}$ at $k = 0.001\ a_0^{-1}$ for MP and static calculations are also reported. PO values are taken from Green *et al.* [14]. MBPT96 and MBPT14 values are thermal averages. Values of $Z_{\rm eff}$ listed are numerically accurate to all quoted digits.

	He	Ne	Ar	Kr	Xe
$Z_{\rm eff}(k = 0.001)$					
Static	0.6887	0.9793	0.7504	0.7035	0.6521
MP	3.997	6.148	31.98	95.10	2444
$\langle Z_{\rm eff}\rangle_T$ (MP)	3.940	6.003	26.77	65.70	401.0
Experimental					
UCSD [5,6]			33.8	90.1	401
UCL [54,55]	3.94 ± 0.02	5.99 ± 0.08	26.77	65.7 ± 0.3	320 ± 5
MBPT96 (1996) [15]	3.94	6	37	65	<320
MBPT14 (2014) [14]	3.79	5.56	26.75	69.66	440.2
Kohn [17]	3.88 ± 0.01				
PO [7–11]		6.98	30.5	56.3	202

orbital energies were calculated using the existing Slater-type basis [53]. The usage of a single value of $G_{\rm core}$ for each atom will lead to overestimation of the annihilation rates for the deeper core subshells in Ar, Kr, and Xe. But these subshells make a very small contribution to the total annihilation rate.

The valence enhancement factors, $G_{\rm val}$ were set by normalizing to experimental estimates of $Z_{\rm eff}$ at thermal energies (once the values $G_{\rm core}$ were fixed). One uncertainty lies in the choice of the experimental values of $\langle Z_{\rm eff}\rangle_T$. These are typically obtained at room temperature so an average of $Z_{\rm eff}(k)$ over a Maxwell-Boltzmann distribution should be used in the comparison of theory and experiment. There are two classes of experiments that are typically used to determine the thermally averaged annihilation parameter $\langle Z_{\rm eff}\rangle_T$. In a traditional experiment, high-energy positrons from a source are injected into a gas, and $\langle Z_{\rm eff}\rangle_T$ is determined from the time decay of the annihilation intensity after the positrons have thermalized [54,55]. In a buffer gas experiment, pioneered by the UCSD group [5,6], positrons are first cooled in a buffer gas such as N_2, and once the positrons have thermalized, the buffer gas is removed and replaced by the target gas and $\langle Z_{\rm eff}\rangle_T$ is measured. The two types of experiment typically give different values of $\langle Z_{\rm eff}\rangle_T$ for the same gas, with the trap configuration typically giving the higher positron annihilation rates. This is noticeable in Table III, where $\langle Z_{\rm eff}\rangle_T$ is tabulated for the noble gases. The present thermally averaged results are determined at $T = 293$ K. This corresponds to a mean positron kinetic energy of $3k_{\rm B}T/2 = 0.0379$ eV, where $k_{\rm B}$ is the Boltzmann constant.

Another uncertainty of the traditional experiments relates to the thermalization of the positrons. Incomplete thermalization would lead to experimental estimates of $\langle Z_{\rm eff}\rangle_T$ being systematically too small. However, experiments for Ar with a small addition of a molecular gas such as H_2 to improve thermalization would be expected to be immune from thermalization issues [55,56]. The experiments with admixtures of molecular gases for Ar still yield values of $\langle Z_{\rm eff}\rangle_T$ that are significantly smaller than those of the UCSD group. On the other hand, the $\langle Z_{\rm eff}\rangle_T$ for xenon with small admixtures of He or H_2 did result in a 20%–30% increase in the xenon $\langle Z_{\rm eff}\rangle_T$.

The $\langle Z_{\rm eff}\rangle_T$ values of the UCL group [54,55,60] were used to fix $G_{\rm val}$ for He, Ne, Ar, and Kr. For xenon, the enhancement factor was tuned to the UCSD $\langle Z_{\rm eff}\rangle_T$ [6]. The enhancement factors, $G_{\rm val}$, adopted in the present calculations are listed in Table II. There is a tendency for $G_{\rm val}$ to increase as the ionization potential of the atom decreases, with the exception being He. Electrons in tightly bound orbitals tend to move in a strong nuclear Coulomb field and this inhibits the ability of the positron to attach these electrons to a cluster resembling the ground state of positronium [49,61].

Beside the experimental values of $\langle Z_{\rm eff}\rangle_T$, there are also some theoretical values listed in Table III. There have been three MBPT calculations [14–16]. The values from MBPT96 [15] and MBPT14 [14] for $\langle Z_{\rm eff}\rangle_T$ were set by performing a convolution with a Maxwell-Boltzmann distribution. The Kohn variational results given by Van Reeth *et al.* [17] was $\langle Z_{\rm eff}\rangle_T$ at 300 K. The PO values of $\langle Z_{\rm eff}\rangle_T$ were given at $k = 0.045\ a_0^{-1}$, referenced from Green *et al.* [14]. The fact that the present value of $Z_{\rm eff}$ at $k = 0.001\ a_0^{-1}$ for xenon is much larger than the $\langle Z_{\rm eff}\rangle_T$ at $T = 293$ K indicates that the $Z_{\rm eff}$ for xenon shows a sharp decrease as the positron momentum increases. This is expected due to the large scattering length [15].

One assumption in our treatment is that the enhancement factors are independent of the recoil momentum. Examination of the annihilation profiles for the e^+He($^3S^e$) metastable state revealed that the annihilation profile for annihilation with the $He^+(1s)$ core were the same (up to a multiplying factor) for a fixed core and full three-body treatment of this system [18]. The enhancement factor also varies slowly as the positron collision energy increases from $E = 0$ [24,41,43,44]. In addition, the integral in Eq. (5) would also tend to smear out any momentum variation of the enhancement factor.

E. Relativistic case

The momentum-space wave functions of heavy rare gases such as xenon are known to be sensitive to relativistic effects [62,63]. Relativistic effects in the γ spectrum were incorporated using an approach adopted to analyze $(e,2e)$ experiments [63]. The target orbital is described using only the large components of the Dirac-Fock (DF) wave function.

The contribution of each $\Phi_{\ell_\mu s_\mu j_\mu}(r)$ orbital is represented as a linear combination of the ℓs coupled wave function $\Phi_{\ell_\mu m_\ell s_\mu m_s}(r)$, where $j_\mu = \ell_\mu \pm \frac{1}{2}$. The contribution to $\Gamma(\mathbf{q})$ from each individual shell $\Phi_{\mu;\ell_\mu s_\mu j_\mu}(r)$ is then written as

$$\Gamma_{\mu;\ell_\mu s_\mu j_\mu} = \frac{N_\mu}{4\ell_\mu + 2}\Gamma_{\mu;\ell_\mu s_\mu}, \tag{18}$$

where N_μ is the number of electrons in the subshell with total angular momentum j_μ and $\Gamma_{\mu;\ell_\mu s_\mu}$ is the contribution from an orbital with an orbital angular momentum of ℓ_μ.

III. RESULTS

The positron annihilation spectra for the noble gas atoms were calculated at an incident positron momentum of 0.001 a.u. using the MP approach. HF wave functions were used to model the structure of the noble gas atom ground states. In Table IV, the final FWHM values are compared with the measurements [1–4] and theoretical calculations using the PO approach [7–11], a static model [64], the MBPT06 method [16], and an approach based on quantum chemistry techniques [12]. A high-accuracy Kohn variational calculation using a correlated basis set for a positron-helium system [17] is also listed.

The MBPT06 calculation was a very restricted many-body calculation. This calculation only incorporated the effects of electron-positron correlation when calculating the annihilation matrix element. It did not include the many-body effects that lead to the long-range electron-positron polarization interaction that changes the scattering length from positive to negative. The MBPT06 calculation contains the contributions from the two outermost shells for all the atoms (except helium). The contribution from the deeper inner shells is less than 0.01% of the total annihilation rate and the omission of this contribution would alter the FWHM values by less than 1%.

TABLE IV. FWHM values (in units of keV) for positron scattering from noble gases are listed. Theoretical results did not include the detector response and the experimental data had been deconvoluted. The uncertainty of the measurement by the UCSD group [2] is 0.02 keV. Measurements from [1] and [3] are angular correlation measurements with uncertainties of 0.05 mrad (0.013 keV) and 0.5 mrad (0.13 keV), respectively. FWHMs from the static model are the same as earlier calculations using this model [2,16,64] for He, Ne, Ar, and Kr. The earlier static calculations [64] gave an FWHM of 2.06 keV for Xe.

	He	Ne	Ar	Kr	Xe
MP	2.59	3.89	2.80	2.53	2.25
PO [7–11]	2.45	3.73	2.81	2.50	2.22
Experimental					
UCSD [2]	2.50	3.36	2.30	2.09	1.92
UCL [1]	2.63	3.19	2.86	2.65	2.58
Stewart [3]	2.40	3.32	2.61	2.63	2.43
Shizuma [4]	2.01	2.04	1.96		1.69
Wang (PWBA) [12]	2.99	5.14	3.85	4.07	
Static	2.53	3.82	2.65	2.38	2.11
MBPT06 [16]	2.35	3.63	2.55	2.30	1.99
Kohn [17]	2.50				

TABLE V. Annihilation parameter, $Z_{\rm eff}$, and γ-spectrum FWHM (in units of keV) for positron annihilation with helium and neon. Calculations were performed at $k = 0.001\ a_0^{-1}$. Ne enhancement factors for the MP calculation were $G_{\rm val} = 2.813$ and $G_{\rm core} = 1.24$. Values of $Z_{\rm eff}$ and FWHM are numerically accurate to at least 0.1%.

	PWBA		Static		MP	
	$Z_{\rm eff}$	FWHM	$Z_{\rm eff}$	FWHM	$Z_{\rm eff}$	FWHM
			Helium			
$1s$	2.0	2.945	0.689	2.532	3.997	2.588
			Neon			
$1s$	2.0	17.799	0.00515	11.388	0.0146	11.398
$2s$	2.0	3.519	0.215	2.779	1.366	2.815
$2p$	6.0	5.684	0.759	4.271	4.767	4.373
Valence	8.0	4.933	0.974	3.813	6.133	3.889
	10.0	5.167	0.979	3.815	6.148	3.891

A. Helium

The construction of the model to describe the elastic cross section for positron scattering from helium was very similar to that reported in a previous work [65]. However, for reasons of computational convenience, the same polarization potential was used for the s, p, and d partial waves (slightly different cutoff parameters were used in [65]). The cutoff parameter was set by normalization to variational calculations of the s-wave phase shift [66,67] at $k = 0.2\ a_0^{-1}$. The model potential reported by Boyle *et al.* [65] gave a good description of the elastic cross section at low energies and was also able to describe the variation of $\langle Z_{\rm eff}\rangle$ with time as the positron was being thermalized. The cross sections agreed to within a few percent with those from a convergent close coupling (CCC) [68] calculation and the experimental cross sections from the ANU [69] and the University of Kyoto [70] groups.

The evolution of $Z_{\rm eff}$ and the γ-spectrum FWHM for the scattering models of different sophistication are listed in Table V. The calculation is dominated by the $L = 0$ partial wave since the FWHM is computed at $k = 0.001\ a_0^{-1}$, where contributions from the p wave and d wave to the annihilation rate are less than 0.001%.

The γ-spectrum FWHM listed in Table V is 3% larger than the UCSD value [2] and about 1% smaller than the UCL value [1]. The tendency for the present calculations to overestimate the UCSD FWHM and underestimate the UCL FWHM occurs for all the rare gases except neon. The MBPT06 estimate of the FWHM is smaller than the MP and PO values and the UCSD and UCL experimental values. The MBPT06 calculation does not incorporate the physics of the electron-positron polarization interaction and the comparison between the static and the MP calculation suggests that this would increase the MBPT06 FWHM by about 0.06 keV.

B. Neon

The elastic cross section for positron scattering from neon is shown in Fig. 2 and compared with the experimental measurements from the Bielefeld group [71], the University of Bath group [72], and the ANU group [73]. Calculations using the MBPT14 approach [14], the PO method [8], and the

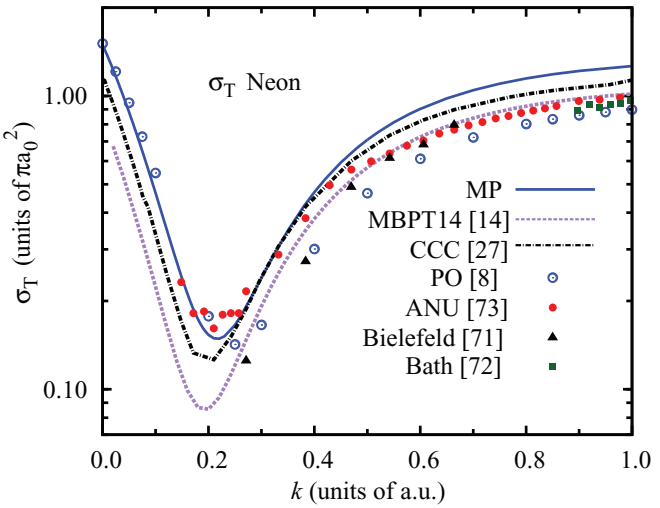

FIG. 2. (Color online) Elastic cross section, $\sigma_T(k)$, for positron scattering from neon.

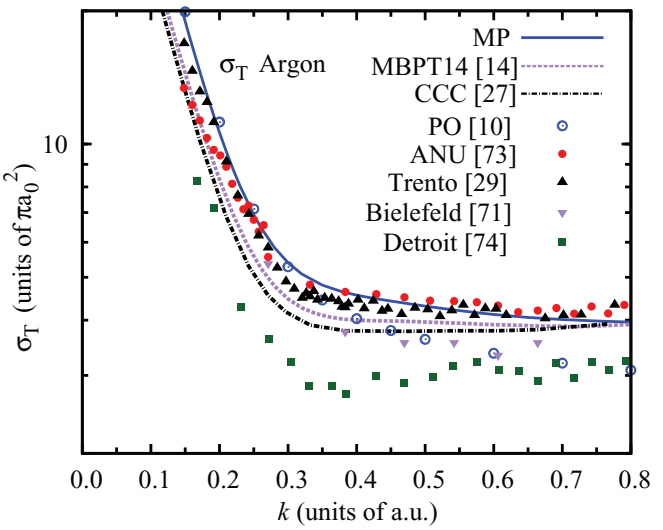

FIG. 3. (Color online) Elastic cross section, $\sigma_T(k)$, for positron scattering from argon. The positronium threshold is at $k = 0.81\ a_0^{-1}$.

CCC method [27] are also depicted. The present calculation was tuned so that its scattering length was the same as that of the PO calculation [8]. The MP cross section provides a reasonable fit to the available experimental data.

The most unusual feature in Fig. 2 is the very small size of the MBPT14 cross section at the Ramsauer minimum. This implies that the MBPT14 p-wave phase shift is significantly smaller than the phase shifts from the other calculations at $k = 0.20\ a_0^{-1}$. The MBPT14 phase shift of 0.0159 rad is significantly smaller than the MP phase shift (0.0193 rad), the PO phase shift (0.0171 rad), and the CCC phase shift ($\approx$0.0177 rad) at this momentum. It should be noted that the PO phase shift is expected to be an underestimate since the dipole polarizability implicit to this model, 2.377 a_0^3, is 14% smaller than the recommended polarizability for neon [24].

Table V lists the individual subshell contributions to $Z_{\rm eff}$ and the FWHM. The contribution from the 1s shell to the total $Z_{\rm eff}$ is very small as expected. The variation of the FWHM upon going from the PWBA to the static model and to the final MP calculation is easily explained. The FWHM is large for the PWBA since the core can make a 20% contribution to the total annihilation rate. The inclusion of the repulsive direct interaction in the static model greatly inhibits the ability of the positron to annihilate with the core 1s subshell. This results in a 30% reduction in the FWHM. The FWHM of the valence orbitals themselves also decreases since the positron does not annihilate with that part of the orbital probability distribution that lies close to the nucleus.

The inclusion of the polarization interaction leads to a slight increase in the FWHM. Two factors could be contributing here. First, the local momentum of the annihilating positron will be larger and this will contribute a slightly higher positron momentum when annihilating with the electrons. The other factor is that the polarization potential allows the positron to penetrate further into the electron charge cloud and, thus, annihilate with the electrons where they are closer to the nucleus and have a higher momentum. It is noticeable that the core makes almost no contribution to the FWHM since the contribution to the total annihilation rate from the core is only 0.3%.

The final MP FWHM, 3.89 keV, is considerably larger than either the UCSD [2] or the UCL [1] measurements. Indeed, all three calculations, MP, PO, and MBPT06, give FWHMs larger than those from the UCL and UCSD experiments. As shown in Table IV , the neon system is the only system where the UCL FWHM is smaller than the UCSD FWHM.

C. Argon

The elastic cross sections in Fig. 3 include experimental measurements from the ANU group [73], the Trento group [29], the Bielefeld group [71], and the Detroit group [74]. Cross sections obtained using the MBPT14 method [14], CCC method [27], and PO method [10] are also shown for comparison.

The MP cross section is compatible with the recent cross sections measured by the ANU and Trento groups. It is worth noting that the replacement of the one-term polarization potential with a three-term potential did lead to an overall improvement in the quality of the agreement at the higher momentum. For example, the one-term model gave an elastic cross section of 2.64 πa_o^2 at $k = 0.8\ a_0^{-1}$, about 50% smaller than the three-term value of 3.96 πa_0^2. There is a reasonable degree of compatibility among the CCC, MBPT14, ANU, Trento, and MP cross sections for $k < 0.25\ a_0^{-1}$. The CCC, MBPT14, and MP cross sections have scattering lengths ranging from -4.3 to $-5.3\ a_0$.

The details of the annihilation spectrum for each subshell of argon are listed in Table VI. The inclusion of the polarization potentials increases $Z_{\rm eff}$ by an order of magnitude. The impact of the enhancement factor in increasing $Z_{\rm eff}$ is about a factor of 3 smaller.

The variations of the FWHM over the various models follow the same pattern as neon. The PWBA FWHM is the largest due to the contribution from the core orbitals. Inclusion of the repulsive direct potential results in the FWHM's decreasing since it leads to a greatly reduced annihilation rate from the

TABLE VI. Annihilation parameter, $Z_{\rm eff}$, and γ-spectrum FWHM (in units of keV) for positron annihilation with argon. Calculations were performed at $k = 0.001\ a_0^{-1}$. Numbers in brackets denote powers of 10.

	PWBA		Static		MP	
	$Z_{\rm eff}$	FWHM	$Z_{\rm eff}$	FWHM	$Z_{\rm eff}$	FWHM
1*s*	2.0	32.718	0.257[−4]	19.647	0.459[−3]	19.647
2*s*	2.0	8.005	0.00237	5.186	0.0422	5.196
2*p*	6.0	16.155	0.00622	9.247	0.111	9.440
3*s*	2.0	2.373	0.136	1.878	6.086	1.953
3*p*	6.0	3.764	0.606	2.886	25.736	3.082
Valence	8.0	3.295	0.742	2.640	31.822	2.793
Total	18.0	3.887	0.750	2.646	31.976	2.795

core orbitals. The total MP FWHM is 20% larger than that measured in the UCSD trap [2] and about 2% smaller than that measured by the UCL group [1].

Once again, the MBPT06 calculation gave the smallest theoretical FWHM, 2.55. The MP FWHM is 0.15 keV larger than the static FWHM. Adding this difference to the MBPT06 would increase it to 2.70 keV, which would be about 15% larger than the UCSD FWHM.

One important origin of uncertainty for positron annihilation rate calculation comes from the description of the correlation effect. We did calculations using the polarization potential with different terms, while the parameters were adjusted to reproduce the scattering length and $Z_{\rm eff}$ that are listed in Table II and Table III. The present three-term calculation predicted an FWHM of 2.795 keV, while the two-term and one-term calculations gave FWHM values of 2.826 and 2.951 keV, which are 1% and 6% larger, respectively.

1. Temperature effects

One advantage of the MP approach is that subsidiary calculations to test various modifications to the calculation can be made very quickly. The effect of finite temperature on the positron can be initially estimated by doing a calculation with the positron momentum set to $k = 0.049\ a_0^{-1}$, which is the mean position momentum for a Maxwell-Boltzmann distribution at 293 K. The resultant FWHM, 2.796 keV, is about 0.1% larger than the $k = 0.001\ a_0^{-1}$ value of 2.795 keV. Thermal effects have a very small effect on the FWHM despite having a considerable impact on the measured $\langle Z_{\rm eff}\rangle_T$.

2. Effect of the core enhancement factor

The use of different enhancement factors for the core and valence electrons has almost no influence on the total annihilation width because the contribution of the core to the total FWHM is very small, contributing 0.002 keV to the total FWHM of 2.795 keV. Using a common enhancement factor for valence and core would result in the FWHM's increasing to 2.799 keV.

3. Effect of the scattering length

The impact of the scattering length on the FWHM was estimated by performing additional calculations with different scattering lengths. The cutoff parameter ρ was adjusted to give scattering lengths to $-4.30\ a_0$ and $-6.30\ a_0$, respectively. The calculations with scattering lengths $-4.30\ a_0$ and $-6.30\ a_0$ predicted FWHM values of 2.769 and 2.819 keV, respectively. A 20% change in the scattering length resulted in a 1% change in the FWHM. The FWHM increased for the $-6.30\ a_0$ calculations since the more attractive polarization interaction allows the positron to penetrate farther into the atomic interior, where the electrons have higher momenta. The small change that does occur is mostly due to the contribution from the valence shell. The change in the scattering length from $-5.28\ a_0$ to $-4.30\ a_0$ and $-6.30\ a_0$ resulted in a 1% change in the FWHM for 3*s* and 3*p* orbitals, while there are only <0.1% changes in the FWHM for the more tightly bound orbitals.

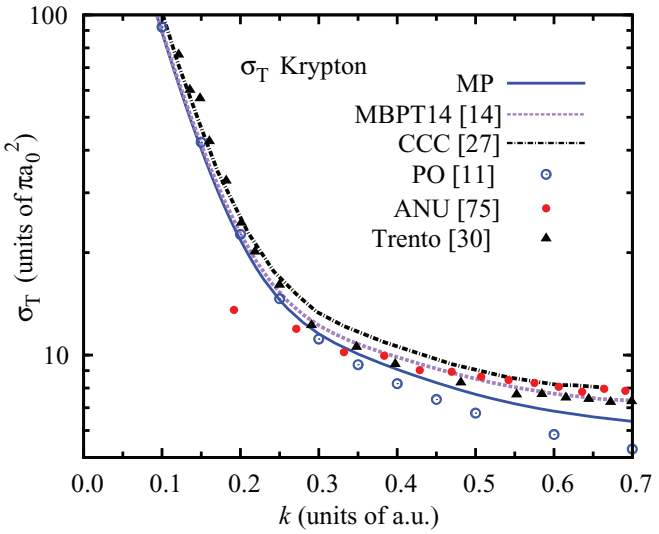

FIG. 4. (Color online) Elastic cross section, σ_T, for positron scattering from krypton as a function of k (in a_0^{-1}). Experimental measurements by the ANU [75] and Trento groups are listed [30]. Theoretical cross sections come from the MBPT14 [14], CCC [27], and PO calculations [11].

D. Krypton

The elastic cross section for positron scattering from krypton are shown in Fig. 4. The present cross sections are compared with the experimental measurements by the ANU group [75] and Trento group [30]. The theoretical results from the MBPT14 calculation [14], CCC calculation [27], and PO calculation [11] are also given for comparison. The lowest energy data point from the ANU group is an outlier and not compatible with a scattering length of $\approx -10\ a_0$.

The orbital contributions to $Z_{\rm eff}$ and the γ-spectrum FWHM for krypton are listed in Table VII. Once again, the MP FWHM of 2.53 keV listed in Table IV is larger than the UCSD value (by 20%) and smaller than the UCL value (by 4%). The contribution of the core to the MP FWHM was only 0.2%. The PO and MP values of the FWHM lie within 1% of each other. The MBPT06 FWHM is 9% smaller than these calculations. However, the change from the static to the MP calculation of the FWHM was 0.15 kev. Adding this as a correction to the MBPT06 FWHM would result in an FWHM of 2.45 keV,

TABLE VII. Annihilation parameter, Z_{eff}, and γ-spectrum FWHM (in units of keV) for positron annihilation with krypton. Numbers in brackets denote powers of 10.

	PWBA		Static		MP	
	Z_{eff}	FWHM	Z_{eff}	FWHM	Z_{eff}	FWHM
1*s*	2.0	66.647	0.115[−6]	38.569	0.593[−5]	38.569
2*s*	2.0	17.852	0.160[−4]	10.734	0.823[−3]	10.742
2*p*	6.0	38.058	0.334[−4]	20.314	0.00171	20.314
3*s*	2.0	6.515	0.00171	4.356	0.0878	4.367
3*p*	6.0	12.014	0.00600	7.655	0.307	7.671
3*d*	10.0	16.654	0.0153	8.853	0.782	8.898
4*s*	2.0	2.116	0.115	1.664	16.888	1.747
4*p*	6.0	3.293	0.565	2.560	77.034	2.761
Valence	8.0	2.915	0.680	2.365	93.921	2.523
	36.0	4.229	0.704	2.378	95.101	2.528

which is only a couple of percent smaller than those of the MP and PO calculations.

E. Xenon

The total elastic cross sections for positron scattering from xenon are shown in Fig. 5. The experimental measurements from the ANU [76] and Trento groups [31] are shown. The theoretical results of the MBPT14 calculation [14], CCC calculation [27], and PO calculation [11] are displayed for comparison. The FWHM and the annihilation parameter Z_{eff} are listed in Table VIII. The MP calculation FWHM is larger than the UCSD value while being smaller than the UCL value. It is noted that the present static model FWHM is 2.5% larger than an earlier calculation using this model [64].

Once again, in order to explore the influence of the polarization potential forms on the FWHM, we did calculations using the polarization potential with different terms. The present three-term calculation predicted an FWHM of 2.253 keV, while the two-term and one-term calculations gave FWHM values of 2.292 and 2.436 keV, which are 2% and 8% larger, respectively.

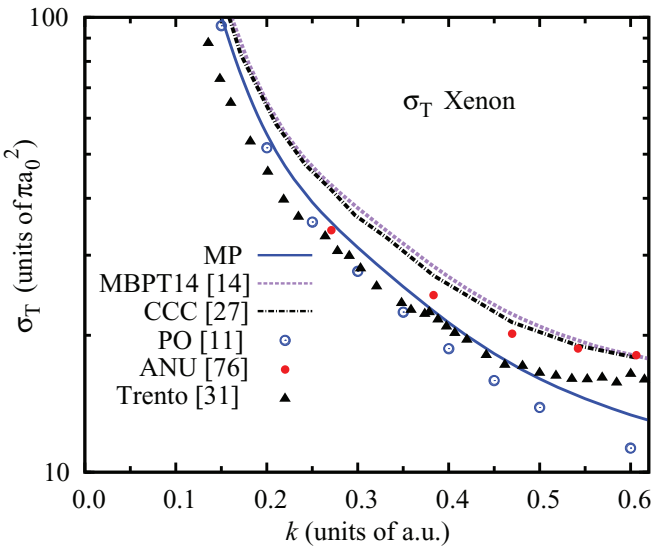

FIG. 5. (Color online) Elastic cross section $\sigma_T(k)$ for positron scattering from xenon.

TABLE VIII. Annihilation parameter, Z_{eff}, and γ-spectrum FWHM (in units of keV) for positron annihilation with xenon. Numbers in brackets denote powers of 10.

	PWBA		Static		MP	
	Z_{eff}	FWHM	Z_{eff}	FWHM	Z_{eff}	FWHM
1*s*	2.0	99.933	0.455[−9]	55.562	0.488[−6]	55.994
2*s*	2.0	27.862	0.848[−7]	16.262	0.910[−4]	16.271
2*p*	6.0	60.120	0.161[−6]	20.858	0.173[−3]	30.858
3*s*	2.0	11.256	0.143[−4]	6.944	0.0153	6.937
3*p*	6.0	21.472	0.423[−4]	12.688	0.0453	12.675
3*d*	10.0	33.963	0.593[−4]	17.372	0.0636	17.377
4*s*	2.0	4.921	0.00158	3.343	1.685	3.358
4*p*	6.0	8.762	0.00636	5.802	6.787	5.829
4*d*	10.0	11.105	0.0230	6.918	24.366	6.973
5*s*	2.0	1.795	0.106	1.435	442.68	1.524
5*p*	6.0	2.835	0.516	2.271	1968.7	2.472
Core	48.0	11.516	0.0310	6.429	32.96	6.472
Valence	8.0	2.511	0.621	2.090	2411.4	2.247
Total	56.0	4.349	0.652	2.109	2444.3	2.253

1. *Relativistic effects*

The impact of relativistic effects on the annihilation spectrum was investigated by replacing the HF wave function for xenon with a DF wave function. Relativistic effects are known to have a measurable effect in electron momentum spectroscopy experiments of the xenon momentum-space wave function [62,63]. The inclusion of relativistic effects resulted in an FWHM that was 1.4% larger, being 2.285 keV, while the HF value was 2.253 keV.

2. *Temperature effects*

Temperature effects were also studied by doing a calculation with the positron momentum set to $k = 0.049\ a_0^{-1}$. The predicted MP value of the FWHM was 2.252 keV. This is very close to the $k = 0.001\ a_0^{-1}$ value, 2.253 keV.

3. *Effect of the core enhancement factor*

The use of different enhancement factors for the core and valence electrons has only a small influence on the total annihilation width because the contribution of the core to the total FWHM is very small, contributing 0.006 keV to the total FWHM of 2.253 keV. Using a common enhancement factor for valence and core would result in the FWHM's increasing to 2.273 keV.

4. *Xenon scattering length*

There is a large variation between the different theoretical and experimental estimates of the xenon scattering length, with values ranging from -45 [11] to $-117\ a_0$ [27]. The value adopted here, $-56\ a_0$, was determined by normalizing the calculated value of $\langle Z_{\text{eff}} \rangle_T$ to the temperature-dependent values measured in the UCSD positron trap [24,32]. The experimental value of $-99(18)\ a_0$ given by the Trento group [31] is

problematic. This is effectively determined by renormalizing the CCC elastic cross section to the experimental data and using the renormalized CCC cross section at 0 energy to determine the scattering length. The implicit assumption was that the momentum dependence of the low-energy cross section was the same for cross sections with significantly different scattering lengths; i.e., cross sections with different scattering rates are the same apart from a scaling factor. There is no justification for this assumption, and it is known that the scattering length has a marked effect on the energy dependence of the low-energy cross section [77,78]. Visual examination of Fig. 5 below $k = 0.4\ a_0^{-1}$ shows that the low-energy experimental cross-section data of the Trento group are about the same size as or smaller than the MP cross section, which has a scattering length of $-56\ a_0$. The Trento data should be larger than the MP cross section here in order to justify the scattering length of $-99\ a_0$.

The most recent MBPT14 calculation of the Belfast group gives a value of $-84.5 \pm 2.0\ a_0$ [14]. This value should be treated as having a significant uncertainty, as it is derived by fitting to a modified effective range theory expression for the low-energy phase shift

$$k\cot(\delta) = -\frac{1}{A} + \frac{\pi\alpha_d k}{3A^2} + \frac{4\alpha_d k^2}{3A}\ln\left(\frac{Ck\sqrt{\alpha_d}}{4}\right) + Dk^3 \tag{19}$$

at $k = 0.02$, 0.04, and 0.06 a_0^{-1}. The constant A is the scattering length, and C and D are additional adjustable parameters. However, the very large scattering length does introduce uncertainties with respect to the validity of this expression for $k \geqslant 0.02\ a_0^{-1}$, the momentum range used in the determination of the MBPT14 scattering length. For example, tuning the current model potential to the MBPT14 phase shift at $k = 0.02\ a_0^{-1}$ leads to a scattering length of $-93\ a_0$.

Additional calculations with the scattering length set to be $-45a_0$ and $-70\ a_0$, respectively, were also performed to explore the impact of the scattering length upon the FWHM. The FWHM predicted with the scattering lengths of $-45\ a_0$ and $-70a_0$ were 2.246 and 2.259 keV, respectively, which are within 0.3% of the present MP value of 2.253 keV.

F. Core annihilation

The UCSD group have measured the γ profile at high Doppler energies and attempted to identify that part of the spectrum that could be ascribed to core annihilation [64]. The UCSD annihilation profile was compared with a calculation using a simple static model to identify the inner-shell contributions. They concluded that the contribution from core electron annihilation had been unambiguously identified for xenon and that their static calculation tended to overestimate the core annihilation rate. The static calculation made a core contribution of 4.8% to the total annihilation rate at $k = 0$ a_0^{-1}. This was halved to 2.4% in order to fit the experimental γ spectrum. This profile is shown in Fig. 6 as the curve labeled "static97." There was a considerable normalization correction applied to the static calculation to achieve this agreement. The $k = 0.001\ a_0^{-1}$ static value of $Z_{\rm eff}$ is smaller than the MP value (which has been normalized to experiment) in Table VIII by a factor of 1000! The initial analysis of the UCSD experiment overstated the case that core annihilation was unambiguously identified.

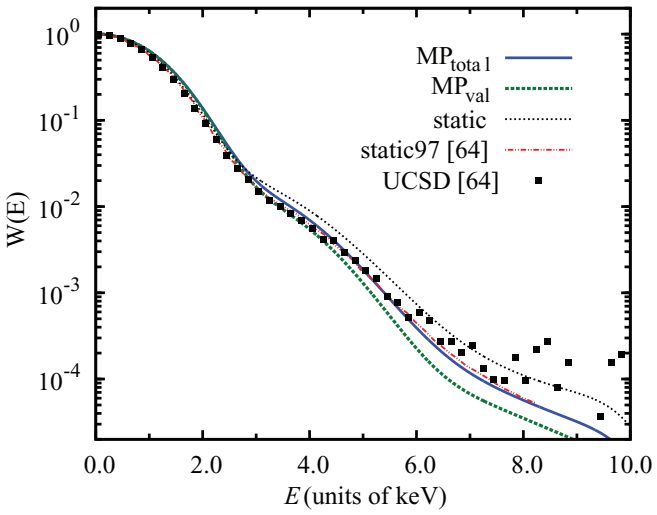

FIG. 6. (Color online) Doppler broadened γ spectrum for positron annihilation on xenon. The present MP and static calculations are presented along with the UCSD experiment [64]. The curve labeled static97 is a static calculation, but with the contribution from the core reduced from 4.8% to 2.4% [64]. Theoretical spectra have been convoluted with the detector response. Two MP curves are shown, one allowing for annihilation from all electrons (MP$_{\rm total}$) and the other excluding core annihilation (MP$_{\rm val}$). The annihilation profile for the static calculation includes core annihilation. All plots are normalized to have the same value at $E = 0$.

Figure 6 depicts a number of calculations of the xenon γ spectrum and compares them with experiment [64]. The plots of the different calculations are all convoluted with the detector response for comparison with experiment [2,64]. The FWHM of the detector response is 1.16 keV. There is a tendency for the static calculation to overestimate the UCSD profile for $E > 3$ keV. The MP calculation tends to follow the UCSD data well up to 6 keV, and after that the UCSD data start to exhibit irregularities. The MP does tend to be slightly larger than the UCSD experiment for E between 1 and 4 keV. This is expected since the MP value of the FWHM is about 15% larger than the UCSD value. The MP$_{\rm val}$ calculation excluding core annihilation only starts to show discernible differences from the full MP calculation for $E > 4$ keV. Figure 7 shows the contributions of the $5s$, $5p$, $4s + 4p + 4d$, and $3s + 3p + 3d$ subshells to the γ spectrum. The contribution from the $n = 4$ subshells only starts to become apparent for $E > 4$ keV.

The annihilation profile is insensitive to relativistic effects in the structure of the target atom. The normalized annihilation profile shows only a small variation when the HF orbitals are replaced by approximate DF orbitals. At $E = 5$ keV, the HF profile is 0.001282, while the DF profile is 0.001310. Such a difference would be barely visible on the logarithmic scale in Fig. 6.

The MP calculation with differential enhancement factors does a much better job of replicating the UCSD γ profile than the static calculation. The omission of core annihilation would result in the MP calculation's underestimating the UCSD spectrum by 47% at $E = 6$ keV.

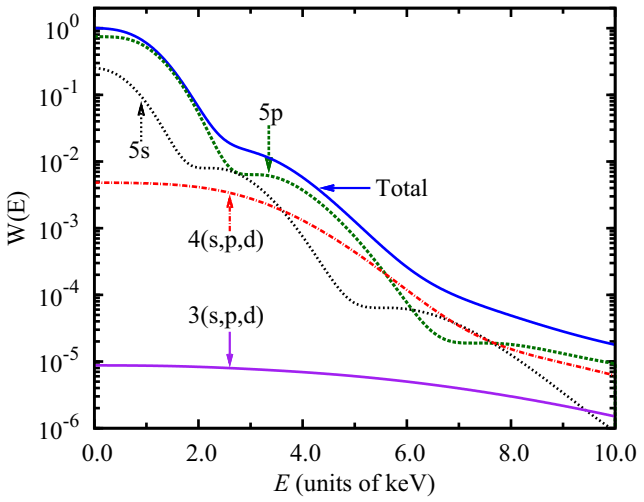

FIG. 7. (Color online) Orbital contributions to the Doppler broadened γ spectrum for positron annihilation on xenon. The spectrum was calculated in the MP model. All data were normalized with the condition that the annihilation rate including all electrons has the value of 1 at $E = 0$.

IV. SUMMARY

MP calculations of the γ-annihilation spectra for positron scattering with rare gas atoms have been performed. While a detailed description of the low-energy elastic cross section was not a primary aim, the adoption of a three-term polarization potential did result in an improved agreement with most recent experiments [29–31,69,73,75,76]. This analysis does suggest that a recent estimate of the Xe scattering length [31] cannot be justified.

The calculated FWHM values were generally a few percent larger than those of the UCSD experiment [2] while being smaller than those determined by the UCL group [1]. We have investigated the impact of the scattering length on the FWHM. The FWHM changed by about 1% for 20% changes in the scattering length. Indeed, the net change in the FWHM from the static calculation (scattering length $= 1.92\ a_0$) to the MP calculation (scattering length $= -56\ a_0$) was only 10%. The calculated FWHM was relatively insensitive to the scattering dynamics of the electron-atom collision.

Similarly, the impacts of finite temperature resulted in a $<1\%$ change from the $k = 0.001\ a_0^{-1}$ value. The annihilation of core electrons also had a small effect on the FWHM. The effect is largest for xenon, but even there the impact was $<1\%$. The FWHM was also insensitive to the use of a relativistic description of the target atom electron density. The FWHM was amazingly stable against changes in the scattering potential and the representation of the target wave function.

The one assumption in the present model that cannot be tested concerns the enhancement factors. The enhancement factor is assumed to be the same for ns and np orbitals. Enhancement factors are known to decrease as the ionization energy of the orbital increases [15,24,35,50]. There is also a possible dependence on the orbital angular momentum of the annihilating electron. Low-energy positrons in the s wave can excite the electron in an ns orbital into a virtual Ps($1s$) state that increases the annihilation rate. This is not true for np orbitals. Either the internal or the center-of-mass angular momentum of the virtual positronium state should be in a p wave. This could act to decrease the enhancement factor. However, the np valence orbitals have lower binding energies than the ns valence orbital, which could act to increase the enhancement factor. A high-quality calculation with a first-principles treatment of electron-positron annihilation will probably be necessary to resolve the issue.

It is difficult to draw any definite conclusions regarding the different values between theory and experiment. With the exception of helium, the MP and PO calculations give roughly the same FWHM. The MBPT06 calculation does give smaller values of the FWHM, but comparisons between the static and the MP FWHM suggest that much of the difference would be removed if the electron-positron polarization interaction was included in the scattering calculation. The different theories tend to give estimates of the FWHM that lie between the UCSD and the UCL experiments, generally being closer to the UCL FWHM for Ar, Kr, and Xe.

The MP calculation does a reasonable job of reproducing the UCSD γ spectrum for xenon at the larger Doppler shifts. It can be regarded as giving a more reliable verification of the core annihilation signal than that originally presented [64]. However, this identification should be treated with caution since the calculation gives an FWHM that is 20% larger than the UCSD value.

ACKNOWLEDGMENTS

The authors would like to thank Gleb Gribakin, D. G. Green, Cliff Surko, James Danielson, and Dmitry Fursa for providing data in tabular form. This work was partially supported under the Australian Research Council's (ARC) Centre of Excellence program. The work of Y.C. was supported in part by National Natural Science Foundation of China Grant No. 11304063.

[1] P. G. Coleman, S. Rayner, F. M. Jacobsen, M. Charlton, and T. L. West, J. Phys. B **27**, 981 (1994).
[2] K. Iwata, R. G. Greaves, and C. M. Surko, Phys. Rev. A **55**, 3586 (1997).
[3] A. T. Stewart, C. V. Briscoe, and J. J. Steinbacher, Can. J. Phys. **68**, 1362 (1990).
[4] K. Shizuma, M. Nishi, T. Fujita, and Y. Yoshizawa, J. Phys. Soc. Japan **44**, 1757 (1978).
[5] K. Iwata, R. G. Greaves, T. J. Murphy, M. D. Tinkle, and C. M. Surko, Phys. Rev. A **51**, 473 (1995).
[6] T. J. Murphy and C. M. Surko, J. Phys. B **23**, L727 (1990).
[7] R. P. McEachran, D. L. Morgan, A. G. Ryman, and A. D. Stauffer, J. Phys. B **10**, 663 (1977).
[8] R. P. McEachran, A. G. Ryman, and A. D. Stauffer, J. Phys. B **11**, 551 (1978).

[9] R. P. McEachran, D. L. Morgan, A. G. Ryman, and A. D. Stauffer, J. Phys. B **11**, 951 (1978).
[10] R. P. McEachran, A. G. Ryman, and A. D. Stauffer, J. Phys. B **12**, 1031 (1979).
[11] R. P. McEachran, A. D. Stauffer, and L. E. M. Campbell, J. Phys. B **13**, 1281 (1980).
[12] F. Wang, L. Selvam, G. F. Gribakin, and C. M. Surko, J. Phys. B **43**, 165207 (2010).
[13] F. Wang, X. Ma, L. Selvam, G. Gribakin, and C. M. Surko, New J. Phys. **14**, 085022 (2012).
[14] D. G. Green, J. A. Ludlow, and G. F. Gribakin, Phys. Rev. A **90**, 032712 (2014).
[15] V. A. Dzuba, V. V. Flambaum, G. F. Gribakin, and W. A. King, J. Phys. B **29**, 3151 (1996).
[16] L. J. Dunlop and G. F. Gribakin, J. Phys. B **39**, 1647 (2006).
[17] P. Van Reeth, J. W. Humberston, K. J. Iwata, R. J. Greaves, and C. M. Surko, J. Phys. B **29**, L465 (1996).
[18] G. G. Ryzhikh and J. Mitroy, J. Phys. B **32**, 4051 (1999).
[19] J. W. Humberston and J. B. Wallace, J. Phys. B **5**, 1138 (1972).
[20] S. E. A. Wakid and R. W. LaBahn, Phys. Rev. A **6**, 2039 (1972).
[21] J. W. Humberston, J. Phys. B **7**, L286 (1974).
[22] Y. K. Ho, J. Phys. B **16**, 1503 (1983).
[23] J. T. Dunn, P. Van Reeth, J. W. Humberston, and G. Peach, J. Phys. B **33**, 2589 (2000).
[24] J. Mitroy and I. A. Ivanov, Phys. Rev. A **65**, 042705 (2002).
[25] J. W. Humberston, Adv. At. Mol. Phys. **15**, 101 (1979).
[26] P. A. Fraser, Adv. At. Mol. Phys. **4**, 63 (1968).
[27] D. V. Fursa and I. Bray, New J. Phys. **14**, 035002 (2012).
[28] R. I. Campeanu and J. W. Humberston, J. Phys. B **10**, L153 (1977).
[29] A. Zecca, L. Chiari, E. Trainotti, D. V. Fursa, I. Bray, A. Sarkar, S. Chattopadhyay, K. Ratnavelu, and M. J. Brunger, J. Phys. B **45**, 015203 (2012).
[30] A. Zecca, L. Chiari, E. Trainotti, D. V. Fursa, I. Bray, and M. J. Brunger, Eur. Phys. J. D **64**, 317 (2011).
[31] A. Zecca, L. Chiari, E. Trainotti, and M. J. Brunger, J. Phys. B **45**, 085203 (2012).
[32] C. Kurz, R. G. Greaves, and C. M. Surko, Phys. Rev. Lett. **77**, 2929 (1996).
[33] M. W. J. Bromley and J. Mitroy, Phys. Rev. A **67**, 062709 (2003).
[34] G. F. Gribakin and J. Ludlow, J. Phys. B **35**, 339 (2002).
[35] S. A. Novikov, M. W. J. Bromley, and J. Mitroy, Phys. Rev. A **69**, 052702 (2004).
[36] J. Mitroy, M. W. J. Bromley, and G. G. Ryzhikh, J. Phys. B **35**, R81 (2002).
[37] J. Mitroy, J. Y. Zhang, M. W. J. Bromley, and S. I. Young, Phys. Rev. A **78**, 012715 (2008).
[38] G. Maroulis and A. J. Thakkar, J. Chem. Phys **89**, 7320 (1988).
[39] D. E. Woon and T. H. Dunning, Jr., J. Chem. Phys. **100**, 2975 (1994).
[40] A. J. Thakkar, H. Hettema, and P. E. S. Wormer, J. Chem. Phys. **97**, 3252 (1992).
[41] G. K. Ivanov, Dokl. Akad. Nauk. SSSR **291**, 622 (1986) [Dokl. Phys. Chem. **291**, 1048 (1986)].
[42] E. Boronski and R. M. Nieminen, Phys. Rev. B **34**, 3820 (1986).
[43] G. F. Gribakin, Phys. Rev. A **61**, 022720 (2000).
[44] G. F. Gribakin and J. Ludlow, Phys. Rev. A **70**, 032720 (2004).
[45] J. Mitroy, Aust. J. Phys. **48**, 893 (1995).
[46] A. K. Bhatia, R. J. Drachman, and A. Temkin, Phys. Rev. A **9**, 223 (1974).
[47] G. G. Ryzhikh and J. Mitroy, J. Phys. B **33**, 2229 (2000).
[48] G. G. Ryzhikh, J. Mitroy, and K. Varga, J. Phys. B **31**, 3965 (1998).
[49] J. Mitroy, M. W. J. Bromley, and G. G. Ryzhikh, J. Phys. B **32**, 2203 (1999).
[50] D. G. Green and G. F. Gribakin, Phys. Rev. A **88**, 032708 (2013).
[51] J. Mitroy and B. Barbiellini, Phys. Rev. B **65**, 235103 (2002).
[52] J. Mitroy, Phys. Rev. A **72**, 062707 (2005).
[53] E. Clementi and C. Roetti, At. Data Nucl. Data Tables **14**, 177 (1974).
[54] P. G. Coleman, T. C. Griffith, G. R. Heyland, and T. L. Killeen, J. Phys. B **8**, 1734 (1975).
[55] G. L. Wright, M. Charlton, T. C. Griffith, and G. R. Heyland, J. Phys. B **18**, 4327 (1985).
[56] I. Al-Qaradawi, M. Charlton, I. Borozan, R. Whitehead, and I. Borozan, J. Phys. B **33**, 2725 (2000).
[57] A. Kumar and W. J. Meath, Mol. Phys. **54**, 823 (1985).
[58] Z. C. Yan, J. F. Babb, A. Dalgarno, and G. W. F. Drake, Phys. Rev. A **54**, 2824 (1996).
[59] J. Mitroy and J. Y. Zhang, Phys. Rev. A **76**, 032706 (2007).
[60] M. Charlton, Rep. Prog. Phys. **48**, 737 (1985).
[61] G. G. Ryzhikh and J. Mitroy, J. Phys. B **31**, 5013 (1998).
[62] J. P. D. Cook, J. Mitroy, and E. Weigold, Phys. Rev. Lett. **52**, 1116 (1984).
[63] J. P. D. Cook, I. E. McCarthy, J. Mitroy, and E. Weigold, Phys. Rev. A **33**, 211 (1986).
[64] K. Iwata, G. F. Gribakin, R. G. Greaves, and C. M. Surko, Phys. Rev. Lett. **79**, 39 (1997).
[65] G. J. Boyle, M. J. E. Casey, R. D. White, and J. Mitroy, Phys. Rev. A **89**, 022712 (2014).
[66] P. Van Reeth and J. W. Humberston, J. Phys. B **32**, 3651 (1999).
[67] J. Y. Zhang and J. Mitroy, Phys. Rev. A **83**, 022711 (2011).
[68] H. Wu, I. Bray, D. V. Fursa, and A. T. Stelbovics, J. Phys. B **37**, L1 (2004).
[69] J. P. Sullivan, C. Makochekanwa, A. Jones, P. Caradonna, and S. J. Buckman, J. Phys. B **41**, 081001 (2008).
[70] T. Mizogawa, Y. Nakayama, T. Kawaratani, and M. Tosaki, Phys. Rev. A **31**, 2171 (1985).
[71] G. Sinapius, W. Raith, and W. G. Wilson, J. Phys. B **13**, 4079 (1980).
[72] P. M. Jay and P. G. Coleman, Phys. Rev. A **82**, 012701 (2010).
[73] A. C. L. Jones, C. Makochekanwa, P. Caradonna, D. S. Slaughter, J. R. Machacek, R. P. McEachran, J. P. Sullivan, S. J. Buckman, A. D. Stauffer, I. Bray *et al.*, Phys. Rev. A **83**, 032701 (2011).
[74] W. E. Kauppila, T. S. Stein, and G. Jesion, Phys. Rev. Lett. **36**, 580 (1976).
[75] C. Makochekanwa, J. R. Machacek, A. C. L. Jones, P. Caradonna, D. S. Slaughter, R. P. McEachran, J. P. Sullivan, S. J. Buckman, S. Bellm, B. Lohmann *et al.*, Phys. Rev. A **83**, 032721 (2011).
[76] J. R. Machacek, C. Makochekanwa, A. C. L. Jones, P. Caradonna, D. S. Slaughter, R. P. McEachran, J. P. Sullivan, S. J. Buckman, S. Bellm, B. Lohmann *et al.*, New J. Phys. **13**, 125004 (2011).
[77] T. F. O'Malley, L. Rosenberg, and L. Spruch, Phys. Rev. **125**, 1300 (1962).
[78] H. A. Bethe, Phys. Rev. **76**, 38 (1949).